NURETH14-401

OBSERVATION OF HIGH HEAT FLUX BOILING STRUCTURES IN A HORIZONTAL POOL BY A TOTAL REFECTION TECHNIQUE

In-Cheol Chu¹, Hee Cheon NO², and Chul-Hwa Song¹

¹ Korea Atomic Energy Research Institute, Daejeon, Korea ² Korea Advanced Institute of Science and Technology, Daejeon, Korea

Abstract

The experiments were carried out for a horizontal pool boiling of saturated water using a transparent ITO heating surface. Details of boiling structure near the heated surface have been clearly observed by applying the total reflection and diagonal view techniques in a synchronized manner. Mechanisms for the bubble coalescence and dry area expansion processes were clearly identified. The base of the large massive bubble was mostly dry with some trapped liquid. The appearance of this large dry area at high heat flux close to CHF was basically resulted from the multiple steps of bubble coalescences which occur while the bubbles are growing, attached to the boiling surface not before they depart from the boiling surface. The thin liquid layer with distributed vapor stems was not observed under the large massive bubble.

Introduction

Owing to the definite importance of the critical heat flux phenomena in many thermal systems, a lot of experiments have been performed to identify the boiling structure at high heat flux condition and the triggering mechanism of the critical heat flux more than several decades. But, the detailed boiling structure near the boiling surface and the CHF mechanism is still controversial even for the simplest case of horizontal pool boiling system. The common observations of the previous visualization works in pool boiling CHF are (1) dry areas appear as the heat flux increases, and the dry areas grow in size and merge with neighboring ones, (2) liquid washes the large dry area after a massive bubble departs from the boiling surface, (3) CHF occurs when the dry area is not wetted but rapidly grows in size. However, the mechanism for the appearance of dry areas and their expansion to larger one is not yet clearly answered, which is the first step to the understanding of the CHF triggering mechanism.

Gaertner [1] took a still shot for a horizontal pool boiling of water, and they postulated the following boiling structure: (1) massive bubble are attached to the surface by numerous columnar stems of vapor, (2) vapor mushroom are planted in the thermal layer and nourished by evaporation at the vapor-liquid interface of the stems, (3) after a mushroom left the surface a new one is immediately established in its place, and the cycle is repeated, (4) close to CHF, the stems collapse due to hydrodynamic instability, causing a local vapor patch to form on the heat-transfer surface.

Kirby and Westwater [2] observed the boiling structure of the horizontal pool boiling of saturated carbon tetrachloride (CCl₄) by applying a bottom-up view to their transparent glass heater. Based on their observation of the bubbles growing within bubble (named Type III bubble), they presumed that (1) a large mass of vapor would be very near the surface, and then a bubble would nucleate in the liquid film beneath the large mass of vapor, thus (2) large vapor patches might grow by evaporating the liquid from this film, and (3) the burnout could be resulted when the liquid film went dry.

Van Ouwerker [3] observed the boiling structure using n-heptane at 101.3, 30, 20 kPa. He described the boiling structure as follows based on the atmospheric condition experiments: (1) when large number of vapor bubbles coalesce near the heating surface at some point they form a large cloud of vapor hovering near the surface, (2) in a thin layer of liquid under the cloud new bubbles nucleate and coalesce with it, (3) from the small dry area which occurs under each of these bubble a tiny dry spot remains in the liquid film under the cloud of vapor, (4) evaporation of the liquid film causes the dry spots to grow and to merge with neighboring ones to form much larger dry areas, (4) when the heat flux is sufficiently large, suddenly at some point on the heating surface a dry area is not wetted and starts growing, leading to burnout.

Gaertner [1], Kirby and Westwater [2], and Van Ouwerker [3] considered or observed the formation of large dry area close to CHF. However, the interpretation of their observation relied on some postulation rather than the direct observation of the detailed boiling structure near the boiling surface. As a result, they commonly came to the conclusion that a thin the evaporation of the liquid film existed under the hovering massive bubble produced the growth of the dry area or the collapse of the columnar vapor steams caused the dry area under the massive bubble.

Haramura and Katto [4] proposed the macrolayer dryout model, considering (1) columnar vapor stems are distributed in a liquid layer wetting a heated surface, (2) the vapor-liquid system is collaped wholly by the Helmholtz instability, but a thin liquid film with vapor stems (*so called*, macrolayer) is left stable on the boiling surface, and (3) CHF appears when the liquid film evaporates away at the end of the hovering time of the massive vapor bubble. On the other hand, Ha and NO [5] proposed the dry spot model with a different view from Haramura and Katto. The basic concepts of the dry spot model are (1) an insulating dry spot forms when the number of bubbles surrounding one bubble exceed a critical number, (2) as the surface temperature is raised, the number of the dry spots increase and the size of dry areas will increase due to merger of several dry spots, and (3) the number of effective nucleation sites will diminish with the increase in the dry area and CHF occurs.

More recently, Nisho et al. [6], and Chung and NO [7] applied the total reflection technique to the horizontal pool boiling of saturated Freon R-113. Later, Nisho and Tanaka [8] extended the total reflection observation to the saturated and subcooled boiling of ethanol and R141b. They commonly reported that (1) dry spots, formed under bubbles, have appeared scattered even at low heat flux nucleate boiling region, (2) the formation of large dry areas results from the coalescence of neighboring dry spots, and (3) the pattern of dry areas at CHF are different from that postulated in the macrolayer dryout model proposed by Haramura and Katto 4]. However, they could not link the dry pattern to the boiling structure (or the dynamic behavior) of the

bubbles on the heating surface. Also, the recording speed of 500 or 1,000 frames per second would not be sufficiently fast to capture the dynamic change of the dry pattern.

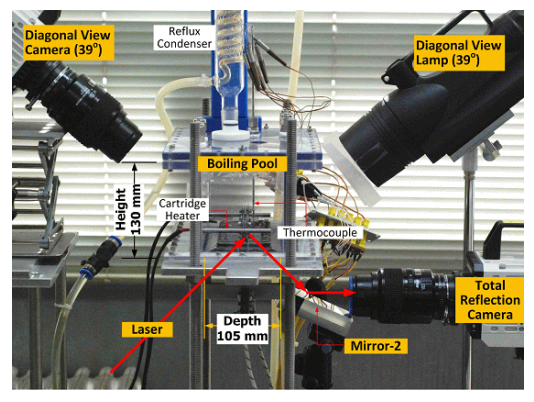
In the present study, visualization experiments were carried out for a horizontal pool boiling of saturated water covering the whole range of nucleate boiling regime from isolated boiling condition to the critical heat flux condition. An in-depth observation of the boiling structure near the boiling surface was made by applying the total reflection and the diagonal view in a synchronized manner. Details of bubble coalescence and dry area expansion processes have been clearly identified.

1. Experimental apparatus and visualization method

The present experimental facility consists of a boiling pool with a transparent heating surface, a power supply system, a data acquisition and control system, a lighting system, and two high speed video cameras. The boiling pool had a cubic shape. The side walls and top plate were made of a transparent polycarbonate plate, and the bottom plate was made of an aluminum plate. A reflux condenser was installed on the top plate of the boiling. The top of the reflux condenser was open to the ambient. As a result, the pressure of the boiling pool was maintained at an atmospheric pressure. Two auxiliary cartridge heaters were inserted through the side wall to control the pool temperature and maintain the pool at a saturated condition. A rectangular sapphire substrate was sit at the central part of the bottom plate. The area and thickness of the sapphire substrate were 80 × 120 mm² and 1 mm, respectively. An ITO (Indium Tin Oxide) layer was used as a heating source because it was not only electro-conductive but also transparent. A 350 nm thick ITO layer was sputtered at the bottom surface of the sapphire substrate. The area of the ITO layer was $8 \times 100 \text{ mm}^2$. The sheet resistance of the ITO layer was approximately 10 Ohm/Sq., and the light transmission rate of the ITO layer was approximately 80% in the visible spectrum. The sapphire substrate sputtered with the ITO was supplied by Diamond Coatings Ltd. Silver electrodes having an area of 8 x 10 mm² were printed on both ends of the ITO layer by Diamond Coatings Ltd. As a result, the heating area of the ITO layer became $8 \times 80 \text{ mm}^2$.

Two identical high speed video (HSV) cameras were used. The HSV cameras are Memrecam GX-3 (color) manufactured by NAC Inc. One was for the total reflection, and the other was for the diagonal view observation. A Xenon HID lamp was installed at the opposite side of the boiling pool. The configuration of the HSV cameras and the lamp is shown in Fig. 1. MICRO NIKKOR 105 mm 1:2.8 lens was installed to each camera. Well synchronized boiling images were obtained from two HSV cameras by providing an external TTL signal to them. In case of the diagonal view observation, the HSV camera and Xenon HID lamp were aligned to have an inclination angle of approximately 39° from the horizon following the suggestion of Bang et al. [9]. In addition, two pyrex windows were installed in parallel to each other in order to maximize the light transmission through the highly agitated interface of coalesced bubble. The window had a thickness of 1 mm and height of 20 mm. The bottom of the window was set to be 0.3 mm above the boiling surface in order to prevent the bubble nucleation at the crevice between the window and the boiling surface, and not to artificially interrupt the continuous liquid supply from both sides of the boiling surface. The distance between the windows was 5.05 mm at the bottom part and 3.2 mm at the top part. The width of ITO layer was also reduced to 2.7 mm for

the length of 14.5 mm at the central region (Fig. 2). The heat flux of the etched ITO region is higher than the region where ITO was not etched. The critical heat flux naturally occurs in the etched region of the ITO layer because the heat flux in the etched region is about 8.8 times higher than the heat flux in the un-etched region.



Window

Massive
Bubble

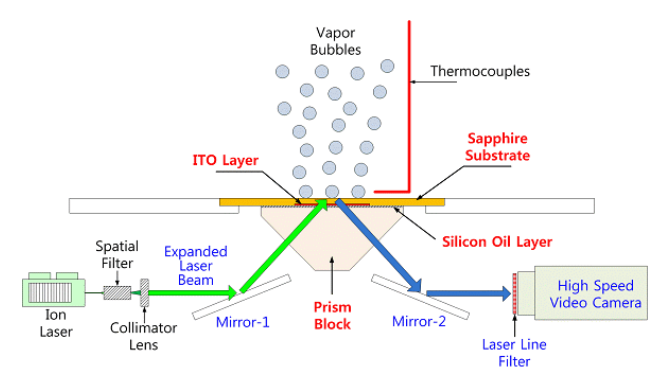
Discrete
Bubble

Discrete
Bubble

Onit: (mm)

Fig. 1 Photo of the test apparatus

Fig. 2 Schematic of the diagonal view arrangement



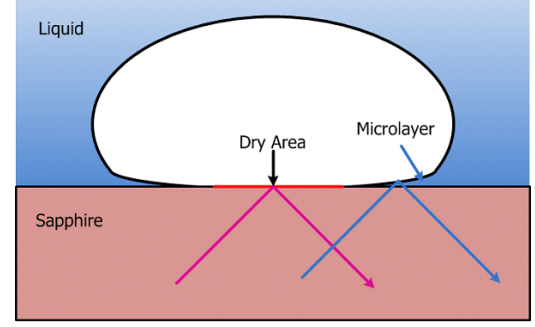


Fig. 3 Schematic of the optical setup for the total reflection

Fig. 4 Schematic of the total reflection from a bubble

Refraction of light bends the light ray toward the tangent to the boundary between the two media when it pass from higher refractive index (n_I) medium to lower refractive index (n_2) medium. The refraction is described by Snell's law which states that no light can pass through and all of the light is reflected back above a certain angle (so called 'critical angle'). This phenomena is the total internal reflection. The optical setup for the present total reflection is schematically illustrated in Fig. 3. A laser beam was incident on the sapphire substrate via the prism block. A prism shaped pyrex block was attached to the ITO layer underneath the sapphire substrate to match the incident angle for the total reflection at the top surface of the sapphire substrate. Silicon oil layer was filled between the top of the prism block and the bottom of the sapphire substrate in order to completely remove the gas phase between them. Otherwise, the total reflection would occur on the top surface of the prism block where gas phase exists. Ion laser with the wavelength of 488 and 514.5 nm was used as a light source for the total reflection.

The laser beam incident on the prism block was inclined approximately 45^o from the horizon in the present experiments. The incident angle was higher than the critical angle at which the total reflection occurs when the top surface of the sapphire was occupied with gas phase. But, the incident angle became lower than the critical angle of the total reflection when the top surface of the sapphire was wetted by liquid. As a result, for nucleate boiling condition, the region where liquid is dried out appears bright in the total reflection image, and the region wetted by liquid appears dark. However, the total reflection can occur at the shallow liquid layer having a smooth gas interface as well as at the dried boiling surface. Therefore, two kinds of total reflections are expected to occur at the base of bubble. One is from the central dry spot, and the other is from the interface between the microlayer and the bubble base, as illustrated in Fig. 4.

The images were recorded at the frame rate of 5,000 fps. The spatial resolutions of these images were (1) 32 μ m (width) and 46 μ m (height) per pixel for the total reflection, and (2) 32 μ m (width) and 73 μ m (height) per pixel for the diagonal view. The shutter speed was 197 μ m (beight) per pixel for the diagonal view and 2 \sim 3 μ m (beight) per pixel for the diagonal view.

2. Experimental results and discussion

2.1 Formation of a dry patch under a coalesced bubble by the merge of individual dry spots

Figure 5 shows the coalescence process of two bubbles at the heat flux of 500 kW/m² (37.2% CHF). The measured CHF in the present tests was 1,345 kW/m². Two bubbles are being generated at 0.0 msec. Two zones of the total reflection are observed for each bubble when they are separated. That is, one is from the central dry area formed by the evaporation of the microlayer, and the other is from the microlayer (Chu et al. [10]). For the bubble in the right side, the total reflection from the left side of the microlayer disappears at 2.0 msec. This implies that the left side microlayer of the right side bubble is agitated by the growth of the bubble in the left side. However, the dry spot of each bubble is intact. Two bubbles collide with each other at 4.0 msec, and start to coalesce at 6.0 msec. After the coalescence of bubbles, two primary dry spots co-exist underneath the coalesced bubble. By evaporating the liquid layer under the coalesced bubble, two primary dry spots expand and they come closer to each other as time goes by.

Figure 6 shows the consecutive images of the synchronized diagonal view and total reflection obtained for the coalescence of three bubbles. The heat flux is 704 kW/m² (52.3% CHF). The number in the first column is the time in millisecond. At time 0.0 msec, the first bubble is growing in the left side of the diagonal view and the total reflection images. At 1.0 msec, the second and the third bubbles grows at the right periphery of the first bubble, and start to coalesce with the first bubble. At 3.0 msec, one bigger bubble is formed from the coalescence of these three bubbles, but three dry spots underneath the coalesced bubble is intact and still separated. The total reflection image at 2.0 msec tells that the right part of the microlayer of the first bubble is disturbed by the growth of the second and the third bubbles. The microlayer under the coalesced bubble evaporates and the dry spots expand due to the heat transfer from the boiling surface, making the separate dry spots get closer. The dry spots corresponding to the first and the second bubbles become connected at 5.0 msec, and all three dry spots become merged into one

bigger dry patch during the time from $7.0 \sim 9.0$ msec. The appearance of the dry patch becomes definitely more frequent with an increase in the heat flux. Afterward, the coalesced bubble and the dry patch behave as follows even though the events are not presented in Fig. 6: the outward expansion of the dry patch mildly continues until approximately 16.4 msec. Then, the coalesced bubble starts to depart from the boiling surface, making the dry patch shrink in its size. The dry patch is totally wetted with the departure of the bubble. The total wetting of the dry patch with the departure of the bubble occurs almost always at this heat flux level even if another new bubble is nucleated around the shrinking dry patch.

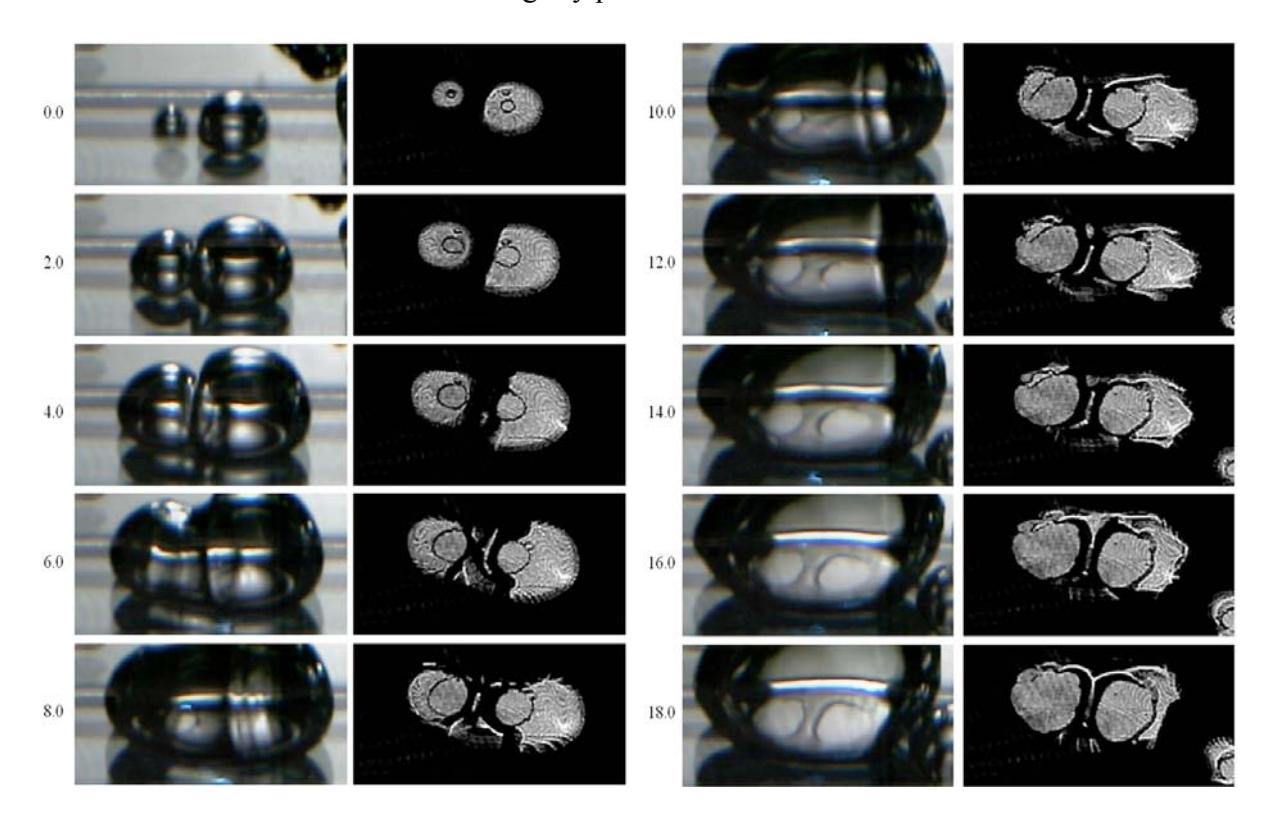


Fig. 5 Consecutive images of the synchronized diagonal view (DV) and total reflection (TR), showing the detailed coalescence process of two bubbles; Heat flux is 500 kW/m^2 (37.2% CHF). Image size is $9.0(\text{W}) \times 9.3(\text{H}) \text{ mm}^2$ for DV, $9.2(\text{W}) \times 5.9(\text{H}) \text{ mm}^2$ for TR. The number left to the images is the time in millisecond.

2.2 Formation of a large dry patch under a large massive bubble by the merge of dry patches

Figure 7 shows the consecutive images of the synchronized diagonal view and total reflection showing (1) the formation of the largest massive bubble resulting in the merge of dry patches into the largest dry patch, and (2) the wetting process of the large dry patch with the depart of the large massive bubble. The heat flux is 1,303 kW/m² (96.9% CHF). The number in the first column is the time in millisecond.

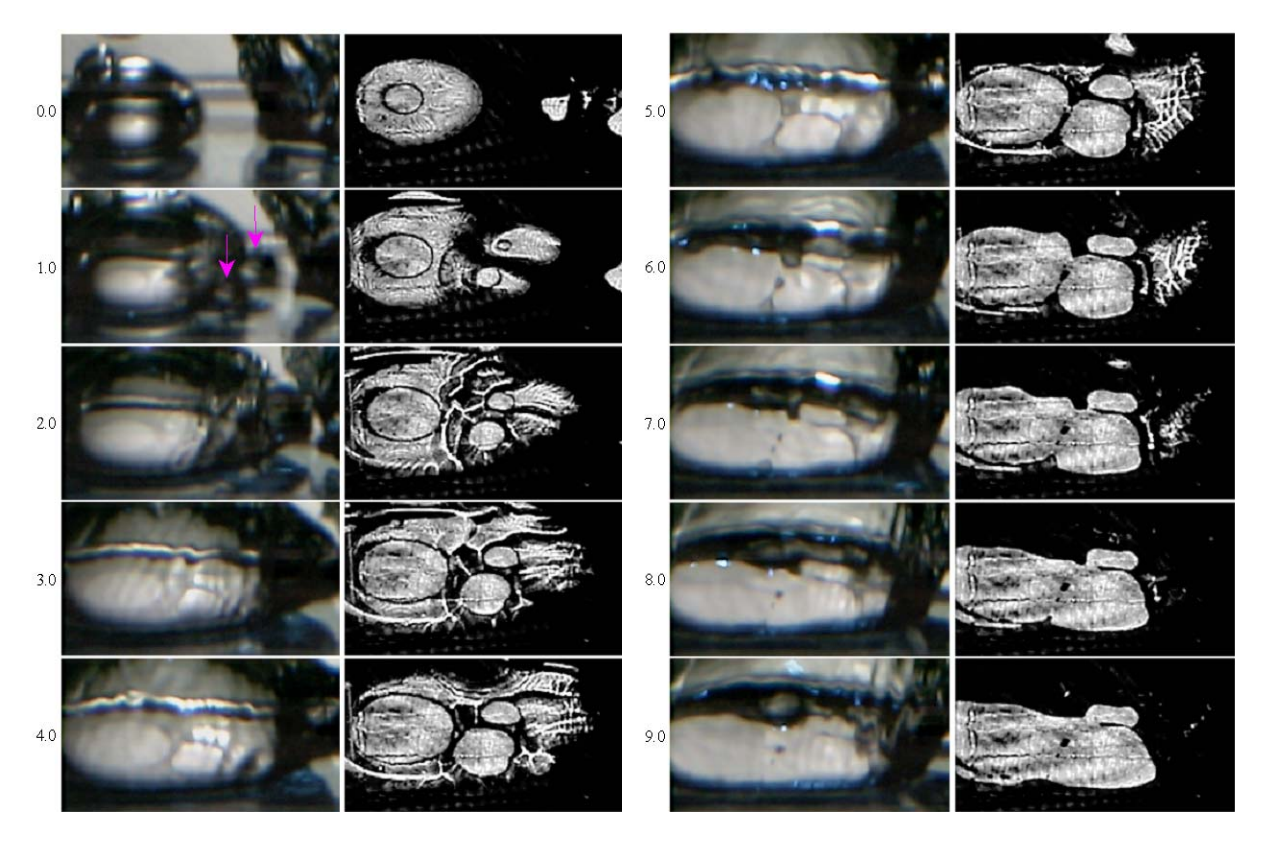


Fig. 6 Consecutive images of the synchronized diagonal view (DV) and total reflection (TR), showing the coalescence of three bubbles and the formation of dry patch by the merge of three dry spots; Heat flux is 704 kW/m^2 (52.3% CHF). Image size is $8.0(\text{W}) \times 9.3(\text{H}) \text{ mm}^2$ for DV, $8.1(\text{W}) \times 5.9(\text{H}) \text{ mm}^2$ for TR. The number left to the images is the time in millisecond.

At 1.0 msec, a dry patch (dry patch No. 1; DP1) was already formed under the massive bubble in the left (massive bubble No. 1; MB1) of the diagonal view and total reflection images, and several bubbles start to coalesce with each other in the right part of the images. At 4.0 msec period, active bubble nucleation occur in the right side of the diagonal view and the total reflection images. The bubbles in the right of the images coalesce with each other during the period of $5.0 \sim 7.0$ msec, which results in the formation of another massive bubble in the right (massive bubble No. 2; MB2). However, the several dry spots under the massive bubble No. 2 are not yet merged. The right part of the dry patch No. 1 recedes due to the expansion of the massive bubble No. 2. At $7.0 \sim 10.0$ msec, a few bubbles are newly generated and they grow between the massive bubbles No. 1 and No. 2. Additionally, the newly growing bubbles make the dry patch No. 1 further recede to the left direction. The newly generated bubbles coalesce with each other, and they produce another large bubble (coalesced bubble No. 1; CB1).

At about 10.0 msec, the massive bubbles No. 1 and No. 2 are bridged by the coalesced bubble No. 1, which triggers the formation of the large massive bubble all across the visualization area. At about 12.0 msec, the dry spots under the massive bubble No. 2 are all merged and produce the second dry patch (dry patch No. 2). About 2.0 msec later, the third dry patch (dry patch No. 3) is formed under the coalesced bubble No. 1 at the center of the images. At about this time, the

large massive bubble is settled all across the visualization area, and three separate dry patches exist underneath the largest massive bubble. The separate dry patches mildly but steadily grow in their size by the evaporation of the trapped liquid among the dry patches until approximately 25.0 msec. As the evaporation of the trapped liquid proceeds, the dry patches No. 2 and No. 3 are merged with each other at 19.0 msec. The dry patch No. 1 is merged with the dry patch No. 2 at 27.0 msec, establishing the single dry patch largest in its area.

The departing motion of the large massive bubble starts from about 25.0 msec, which can be deduced from total reflection images by considering that the total dry area begins to decrease. Differently from the images in Figs. 6, many new bubbles are generated around the periphery of the large massive bubble immediately after the dry patch is partly wetted at this high heat flux of 96.9% (as seen in the images at 27.0 and 51.4 msec). They coalesce with the departing massive bubble at the bottom periphery of the departing bubble. The large massive bubble already departed from the boiling surface at 57.4 msec. Nevertheless, the boiling surface is not completely wetted but partly covered by a small dry patch (*hereafter*, a residual dry patch). The residual dry patch is marked with the circle in the total reflection image at 58.4 msec. The adhesion force of the newly generated bubbles to the boiling surface is higher than that to the departing massive bubble. As a result, (1) the bottom of the departing massive bubble is disconnected from the newly generated bubbles which were previously coalesced with the departing massive bubble at its bottom region, and (2) a part of bubble remains on the boiling surface (*hereafter*, a remaining bubble), which accompanies the residual dry patch.

From 70.8 to 73.8 msec, several bubbles are generated around the residual dry patches which remain on the boiling surface after the departure of the previous massive bubble. At 73.8 msec, two coalesced bubbles (coalesced bubbles No. 2 and No. 3; CB2, CB3) are formed in the left and central regions of the images, respectively. A dry patch (dry patch No. 4; DP4) is formed under the coalesced bubble No. 2, but the dry spots are not yet merged under the coalesced bubble No. 3. Another bubble (bubble No. 1) is generated between the coalesced bubble No. 2 and No. 3 at 73.8 msec. This bubble becomes the bridge between the coalesced bubbles No. 2 and No. 3, as can be seen from the images at 75.8 and 77.8 msec. Another new bubble (bubble No. 2) is growing in the right end of the images even though it is not sure if the bubble is a single bubble or a coalesced one. From 79.8 msec, another large massive bubble (LMB No. 2) is being formed by the coalescence of the coalesced bubbles No. 2 and No. 3, and the bubble No. 1. At 87.8 msec, the large massive bubble is settled again all across the visualization area by the coalescence with the bubble No. 2.

At 83.8 msec, another dry patch (dry patch No. 5; DP5) is formed by the merge of the dry spot of the bubble No. 1 and the dry area under the coalesced bubble No. 3. At 87.8 msec, the large dry patch is formed by the merge of the dry patches No. 4 and No. 5 as these dry patches expand by the evaporation of the liquid between them. Until 93.8 msec, the large massive bubble and the large dry patch exist stably on the boiling surface. The departing motion of the large massive bubble starts a few milliseconds later even though not shown in Fig. 7. The subsequent process until the departure of the largest massive bubble is similar to that shown during the period of $27.0 \sim 58.2$ msec, except that the dry area of the bubble No. 2 in the right remains isolated.



Fig. 7 Consecutive images of the synchronized diagonal view (DV) and total reflection (TR), showing the formation of the large massive bubble resulting in the merge of dry patches into the large dry patch; Heat flux is 1,303 kW/m 2 (96.9% CHF). Image size is 15.2(W) × 11.6(H) mm 2 for DV, 15.4(W) × 7.3(H) mm 2 for TR. The number left to the images is the time in millisecond.

The 14th International Topical Meeting on Nuclear Reactor Thermalhydraulics, NURETH-14 Toronto, Ontario, Canada, September 25-30, 2011

The major events shown in Fig. 7 are as follows:

✓ 1.0 msec: the formation of the dry patch No. 1 under the massive bubble No. 1,

✓ 7.0 msec: the formation of the massive bubble No. 2 by the lateral coalescence of bubbles,

✓ 12.0 msec: the formation of the dry patch No. 2 by the merge of dry spots,

 \checkmark 16.0 msec: the settlement of the large massive bubble by the coalescence of the massive

bubbles, and the existence of several dry patches under the large massive bubble,

 \checkmark 20.0 msec: the merge of the dry patches of No. 2 and No. 3 by the evaporation of the liquid

between them,

✓ 27.0 msec: the merge of all three dry patches under the large massive bubble,

✓ 75.8 msec: the formation of the dry patch No. 4 under the coalesced bubble No. 2,

✓ 83.8 msec: the formation of the dry patch No. 5 by the merge of the separated dry areas

under the coalescing bubbles,

✓ 87.8 msec: the settlement of the large massive bubble mainly by the coalescence of massive

bubbles and the formation of the large dry patch by the merge of the dry patches.

3. Conclusions

Using the transparent ITO heater, the synchronized total reflection and diagonal view observations have been successfully applied to the horizontal pool boiling of saturated water which has the CHF value above 1 MW/m². Details of bubble coalescence and dry area expansion processes were clearly identified.

The mechanism for the appearance of large dry area can be summarized as follows based on the present in-depth observations:

- (1) the base of individual bubble is almost dry (so called, dry spot) by the evaporation of the microlayer,
- (2) individual bubbles coalesce with each other while they are growing (i.e., being still attached to the boiling surface),
- (3) separated dry spots under the coalesced bubble grow and merge by the evaporation of the trapped liquid, which produces a dry patch,
- (4) a large massive bubble is formed by the coalescence of a few massive and/or pre-coalesced bubbles while they are attached to the boiling surface,
- (5) a large dry patch is formed by the merge of separate dry patches and dry spots under the large massive bubble (*i.e.*, the large dry patch under the large massive bubble is basically formed by the multiple steps of bubble coalescences while these bubbles are growing on the boiling surface, not before they depart from the surface).

The present observation supports the basic concept of the dry spot model of Ha and No [5] among several CHF models for pool boiling. However, the macrolayer, which has been considered to exist under a large massive bubble as a thin liquid film with distributed vapor stems, was not observed in the present observation.

4. References

- [1] R.F. Gaetner, "Photographic Study of Nucleate Pool Boiling on a Horizontal Surface", J. Heat Transfer, Vol. 87, 1965, pp. 17-29.
- [2] D. B. Kirby and J. W. Westwater, "Bubble and Vapor Behavior on a Heated Horizontal Plate during Pool Boiling near Burnout", Chem. Eng. Prog. Symp., Vol. 61, 1965, pp. 238-248.
- [3] H. J. Van Ouwerkerk, "Burnout in Pool Boiling the Stability of Boiling Mechanism", Int. J. Heat Mass Transfer, Vol. 15, 1972, pp. 25-34.
- [4] Y. Haramura and Y. Katto, "A New Hydrodynamic Model of Critical Heat Flux, Applicable Widely to Both Pool and Forced Convection Boiling on Submerged Bodies in Saturated Liquid", Int. J. Heat Mass Transfer, Vol. 26, 1983, pp. 389-399.
- [5] S. J. Ha and H. C. NO, "A Dry-spot Model of Critical Heat Flux in Pool and Forced Convection Boiling", Int. J. Heat Mass Transfer, Vol. 41, 1998, pp. 303-311.
- [6] S. Nishio, T. Gotoh, N. Nagai, "Observation of Boiling Structures in High Heat-Flux Boiling", Int. J. Heat Mass Transfer, Vol. 41, 1998, pp. 3191-3201.
- [7] H. J. Chung and H. C. NO, "Simultaneous Visualization of Dry Spots and Bubbles for Pool Boiling of R-113 on a Horizontal Heater", Int. J. Heat Mass Transfer, Vol. 46, 2003, pp. 2239-2251.
- [8] S. Nishio and H. Tanaka, "Visualization of Boiling Structures in High Heat-Flux Pool-Boiling", Int. J. Heat Mass Transfer, Vol. 47, 2004, pp. 4559-4568.
- [9] I. C. Bang, S. H. Change and W.-P. Baek, "Visualization of a Principle Mechanism of Critical Heat Flux in Pool Boiling", Int. J. Heat Mass Transfer, Vol. 48, 2005, pp. 5371-5385.
- [10] I.-C. Chu, C.-H. Song, H. C. NO, "Bubble Growth and Microlayer Evaporation in a Horizontal Pool Boiling of Saturated Water", <u>NTHAS7: The Seventh Korea-Japan</u> <u>Symposium on Nuclear Thermal Hydraulics and Safety</u>, Paper No. N7P0066, Chuncheon, Korea, 2010, November 14- 17.